

# Multiscale Amplitude-Modulation Frequency-Modulation (AM-FM) Texture Analysis of Multiple Sclerosis in Brain MRI Images

C. P. Loizou, *Member, IEEE*, V. Murray, *Member, IEEE*, M. S. Pattichis, *Senior Member, IEEE*, I. Seimenis, M. Pantziaris, and C. S. Pattichis, *Senior Member, IEEE*

**Abstract**—This study introduces the use of multiscale amplitude modulation–frequency modulation (AM–FM) texture analysis of multiple sclerosis (MS) using magnetic resonance (MR) images from brain. Clinically, there is interest in identifying potential associations between lesion texture and disease progression, and in relating texture features with relevant clinical indexes, such as the expanded disability status scale (EDSS). This longitudinal study explores the application of 2-D AM–FM analysis of brain white matter MS lesions to quantify and monitor disease load. To this end, MS lesions and normal-appearing white matter (NAWM) from MS patients, as well as normal white matter (NWM) from healthy volunteers, were segmented on transverse T2-weighted images obtained from serial brain MR imaging (MRI) scans (0 and 6–12 months). The instantaneous amplitude (IA), the magnitude of the instantaneous frequency (IF), and the IF angle were extracted from each segmented region at different scales. The findings suggest that AM–FM characteristics succeed in differentiating 1) between NWM and lesions; 2) between NAWM and lesions; and 3) between NWM and NAWM. A support vector machine (SVM) classifier succeeded in differentiating between patients that, two years after the initial MRI scan, acquired an EDSS  $\leq 2$  from those with EDSS  $> 2$  (correct classification rate = 86%). The best classification results were obtained from including the combination of the low-scale IA and IF magnitude with the medium-scale IA. The AM–FM features provide complementary information to classical texture analysis features like the gray-scale median, contrast, and coarseness. The findings of this study provide evidence that AM–FM features may have a potential role as surrogate markers of lesion load in MS.

**Index Terms**—Amplitude-modulation frequency-modulation (AM–FM), magnetic resonance imaging (MRI), multiple sclerosis (MS), texture analysis.

## I. INTRODUCTION

**M**ULTIPLE sclerosis (MS) is a chronic autoimmune disease that results in multiple areas of inflammatory demyelination within the central nervous system. Within individuals, the clinical manifestations are unpredictable, particularly with regard to the development of disability [1], [2]. MS diagnosis made by a specialized neurologist is primarily based on clinical signs and symptoms, while several paraclinical tests can help in disease verification. Magnetic resonance imaging (MRI) can depict the multifocal lesions in the central nervous system most often associated with MS and, therefore, plays a significant role in detecting disease onset and monitoring disease activity [1]. Many attempts have been made to use MRI to assess disease burden, lesion evolution, correlation with clinical status, as well as treatment effectiveness in MS. Correlations between changes in disability and brain MRI activity have been reported [2], as well as classification of disease subgroups based on brain MRI histograms [3]. On the other hand, conventional MRI techniques, such as T2-weighted imaging tend to depict severe tissue destruction and their outcomes correlate poorly with the clinical status of MS patients and manifested clinical activity [4]. This lack of correlation is mainly due to the presence of additional microscopic abnormalities in the so-called normal-appearing white matter (NAWM) in which T2-weighted imaging fails to unveil. The problem has been termed the clinic-radiological paradox [5]. In addition, conventional MRI methods currently used in MS are not reliable for predicting the clinical evolution of the disease. Thus, there is a need for novel techniques that can lead to improved specificity and sensitivity in diagnosing and monitoring MS [6].

Texture feature analysis can be used to analyze macroscopic lesions and other macroscopic changes in the MS brains that go beyond the conventional measures of lesion volume and number [1]. Texture analysis is also used widely in neuro MRI to enable disease characterization and quantification. Here, texture features are used to detect and quantitatively evaluate not only macroscopic changes but also subtle signal intensity variations. Herlidou-Même *et al.* [7] showed how texture features can reveal discriminant factors for differentiating between normal and abnormal tissue, and also for image segmentation. The use of

Manuscript received April 30, 2010; revised September 20, 2010; accepted October 29, 2010. Date of publication November 9, 2010; date of current version January 4, 2011. This work was supported by the Project “Quantitative and Qualitative Analysis of MRI Brain Images,” under Grant IPF/ORIZO/0308(BIE)/15 dated 12/2008–12/2010, of the Program for Research and Technological Development 2007–2013, Research Promotion Foundation of Cyprus.

C. P. Loizou is with the Department of Computer Science, School of Sciences, Intercollege, CY-3507 Limassol, Cyprus (e-mail: loizou.c@lim.intercollege.ac.cy; panloicy@logosnet.cy.net).

V. Murray and M. S. Pattichis are with the Department of Electrical and Computer Engineering, The University of New Mexico, Albuquerque, NM 87131 USA (e-mail: vmurray@ieee.org; pattichis@ece.unm.edu).

I. Seimenis is with the Medical Diagnostic Center “Ayios Therissos,” 2033 Nicosia, Cyprus (e-mail: yseimen@phys.uoa.gr).

M. Pantziaris is with the Cyprus Institute of Neurology and Genetics, 1683 Nicosia, Cyprus (e-mail: pantzari@cing.ac.cy).

C. S. Pattichis is with the Department of Computer Science, University of Cyprus, 1678 Nicosia, Cyprus (e-mail: pattichi@ucy.ac.cy).

Color versions of one or more of the figures in this paper are available online at <http://ieeexplore.ieee.org>.

Digital Object Identifier 10.1109/TITB.2010.2091279

texture analysis for classification of active and nonactive brain lesions in MS patients from brain MRI was investigated in [8]. Here, it was shown that active lesions could be identified without frequent gadolinium injections, using run length analysis criteria. In [9], the performance of texture analysis concerning discrimination between MS lesions, NAWM, and normal white matter (NWM) from healthy controls was investigated by using linear discriminant analysis. The results suggested that texture features can support early diagnosis in MS. When a combined set of texture features was used [9], similar findings were reported. Significant differences in texture between normal and abnormal spinal cord in MS patients, as well as significant correlation between texture features and disability were found in [10]. The median value increase of these texture features suggests that the lesions texture in MS patients is less homogeneous and more complex than the corresponding healthy tissue (NWM) in healthy subjects [10]. Similar findings were also described in [11] and [12], where it was shown that the median values of lesions texture features, such as standard deviation, median, sum-of-squares variance, contrast, sum average, sum variance, difference variance, and difference entropy increased significantly with the progression of the MS disease when compared to NWM tissue. Statistical analysis has shown (using the spatial gray-level dependence matrices) that there is a significant difference between NAWM, NWM, and lesions. These findings may be beneficial in the research of early diagnosis and treatment decision in MS.

Theodorakis *et al.* [13] developed a pattern-recognition system for the discrimination of MS from cerebral microangiopathy lesions based on computer-assisted texture analysis of MR images. It was shown that, MS regions were darker, of higher contrast, less homogeneous, and rougher as compared to cerebral microangiopathy.

Different-intensity normalization schemes of brain images were investigated in a longitudinal study in [15]. It was shown that significant error reduction could be achieved by applying tissue-specific intensity normalization and partial-volume filtering. It was also shown that different normalization methods and different acquisition protocols influence the texture-analysis results. Image-intensity normalization is also needed for tissue classification [14]. The influence of different MRI acquisition protocols and four gray-level intensity normalization methods on the discrimination power on the texture analysis of two classes of samples were investigated in [15].

To introduce the objectives of our study, an example in Fig. 1 is displayed. Fig. 1(a) and (b) shows two transaxial T2-weighted MR images at the same level of the brain acquired from the same patient. The image in Fig. 1(a) corresponds to the initial diagnosis of a clinical isolated syndrome (CIS) of MS. A second MR scan acquired within the time framework of 6–12 months later is shown in Fig. 1(b). The two delineated regions of interest (ROIs) corresponding to the same MS plaque are also depicted. Fig. 1(c) shows the magnified segmented lesions from Fig. 1(a) and (b) (original images were acquired at a sampling rate of 2.226 pixels/mm). To maintain physical perspective, the bar below the lesions shows the corresponding physical size of

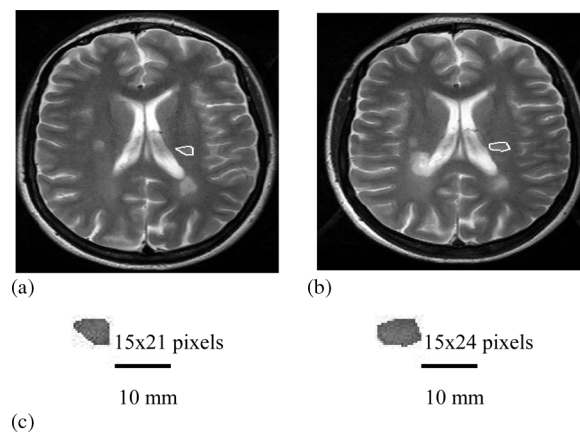


Fig. 1. ROIs drawn on MR images of the brain obtained from an MS patient at (a) 0 and (b) 6–12 months. (c) Magnified segmented lesions from (a) and (b) that are acquired at a pixel resolution of 2.226 pixels/mm. The bar below the lesions shows the size of 10 mm. The image intensity median and interquartile range (IQR) of the segmented lesions at 0 and 6–12 months were 108 and 9.6 versus 99 and 11.8, respectively.

10 mm. In what follows, texture analysis refers to the image processing of the extracted ROIs.

Our primary objective here is to develop new texture classification methods, which can be used to differentiate between MS brain lesions that will develop into advanced disease stages, from lesions that will develop into mild disease stages. This application investigates the use of new multiscale amplitude-modulation frequency-modulation (AM–FM) features extracted from multiple frequency scales [16]–[19]; furthermore, it also investigates the use of multiscale AM–FM features to detect significant differences between NWM and NAWM, as well as for better tissue discrimination between them. Significant differences between NWM and NAWM may be critical to the early diagnosis of the disease, while better tissue discrimination may be valuable as a prognostic factor in the assessment of the natural evolution of the disease. Since the use of quantitative MRI analysis as a surrogate outcome measure in clinical trials presupposes a close relationship between the change in the extracted features and the clinical status, and rate of development of disability, patient images acquired at two different time points were analyzed and AM–FM texture findings with disability assessment scales were correlated.

The promising role of AM–FM methods in medical image analysis can be summarized in that [19]: 1) they provide physically meaningful texture features, over multiple scales, at pixel-level resolution; 2) images can be reconstructed from AM–FM components; 3) AM–FM decompositions can be extracted for different frequency coverage; and 4) the recent development of robust methods for AM–FM demodulation allow for accurate decompositions (see recent examples in [17]). The advantages of the AM–FM approach will become more apparent in Section II.

While there are several studies reported earlier suggesting that the progression of the textural characteristics may be associated with disease progression in MS subjects [7]–[15], [20], no other studies reported in the literature were found, where the AM–FM

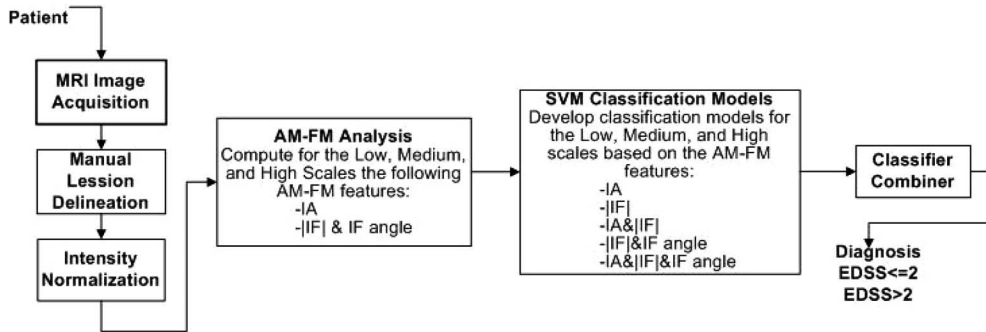


Fig. 2. MRI-image-analysis system diagram.

characteristics (or any other multiscale features) of the brain MRI lesions have been shown to be associated with the disease progression. Preliminary findings of this study, for the AM-FM analysis of NAWM in MS subjects, were also published in [21] and [22]. The use of standard textural features has been presented in [10]–[12].

## II. MATERIALS AND METHODS

The system diagram in Fig. 2 presents the different processing blocks. In what follows, each block will be presented in detail.

### A. Study Group and MRI Acquisition

Thirty-eight patients (17 males, and 21 females), aged  $34.1 \pm 10.5$  (mean age  $\pm$  standard deviation), with a CIS of MS and MRI-detectable brain lesions were scanned twice at 1.5 T with an interval of 6–12 months. The transverse MR images used for the analysis were obtained using a T2-weighted turbo spin-echo pulse sequence (repetition time = 4408 ms, echo time = 100 ms, echo spacing = 10.8 ms). The reconstructed image had a slice thickness of 5 mm and a field of view of 230 mm with a pixel resolution of 2.226 pixels/mm. Standardized planning procedures were followed during each MRI examination.

Initial diagnosis was made by an experienced MS neurologist who referred patients for a baseline MRI upon diagnosis and clinically followed all patients for over two years. All patients remained untreated between the baseline MRI and the repeat MRI. They were also subjected to an expanded disability status scale (EDSS) test two years after initial diagnosis to quantify disability [20]. They were clinically followed and examined by an MS neurologist (coauthor M. Pantziaris) following the initial MRI (time 0) and also at two years later (time 6–12). At the initial scan, the stage of the disease was evaluated using the EDSS score [20]. This gave starting EDSS scores with a mean of 2.07 and a standard deviation of 0.75. The number of subjects with  $EDSS \leq 2$  and  $EDSS > 2$  two years after the first examination were 23 and 15, respectively. Additionally, the brains of 20 healthy, age-matched (mean  $\pm$  SD:  $30.8 \pm 7.6$ ) volunteers (8 males, and 12 females) were MRI-scanned to allow segmentation and analysis of normal brain white matter. The subjects were referred for the MRI scans to Ayios Therissos Medical Diagnostic Center (coauthor, I. Seimenis).

### B. Manual Delineations of the ROIs

All detectable brain lesions were identified and segmented by an experienced MS neurologist and confirmed by a radiologist. Only well-defined areas of hyperintensity on T2-weighted MR images were considered as MS plaques. The neurologist manually delineated (using the mouse) the brain lesions by selecting consecutive points at the visually defined borders between the lesions and the adjacent NAWM on the acquired transverse T2-weighted sections. The manual delineations were performed using a graphical user interface implemented in MATLAB developed by our group. For each brain MRI scan of MS patients, ten discrete round ROIs with an approximate radius of 25 pixels were also drawn in brain white matter, usually contralateral to the lesion side, to represent NAWM. Every effort was made to avoid white matter areas with subtle, patchy, and diffuse abnormal signal intensities. Finally, the neurologist manually segmented cerebrovascular fluid (CSF) areas as well as the areas with air (sinuses) from all MS brain scans. Similarly, ROIs representing NWM, CSF, and air from the sinuses were arbitrarily segmented from the brain scans of the 20 healthy subjects. Manual segmentation by the MS expert was performed in a blinded manner, without the possibility of identifying the subject, the time-point of the exam, or the clinical findings. The selected points and delineations were saved to be used for texture analysis.

### C. Interscan Intensity Normalization

A normalization algorithm adjusts distributions of each follow-up scan to match those of the chosen baseline scan in order to improve image compatibility and facilitate MR image comparability between serial MR scans [14], such as those obtained from the MS group of this study. In a recent study [23], where six different interscan normalization techniques for MRI were compared, it was shown that a normalization method based on histogram normalization proposed in [24], in which the original histogram of the whole image is stretched and shifted in order to cover a wider dynamic range, yields better results than the other methods tested. The original image histogram was stretched, and shifted using the following equation [23], [24]:

$$f(x, y) = \frac{g_{HIR} - g_{LIR}}{g_{max} - g_{min}}(g(x, y) - g_{min}) + g_{LIR} \quad (1)$$

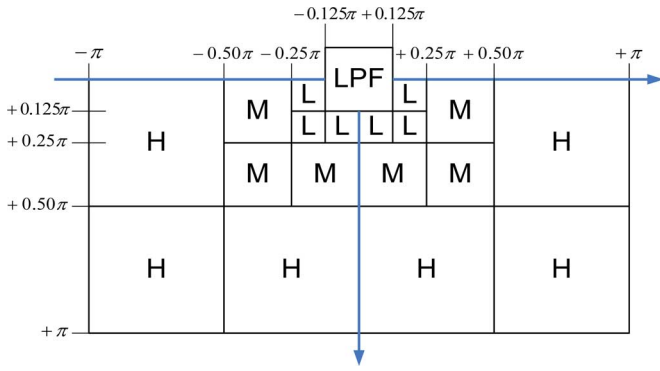


Fig. 3. Spectral coverage of dyadic filterbank showing low-(L), medium-(M), and high-(H) frequency-scale channel filters. Based on the sampling period of 2.226 pixels/mm, we need to multiply the discrete space frequencies of this figure by  $1.113/\pi$  to convert to cycles per millimeter (in each dimension). Due to the inherent symmetry of frequency components for real images, expressed as  $F(u, v) = F^*(-u, -v)$  in the spectral domain, we note that the upper two quadrants can be inferred from the lower ones. See [18] for details on the method.

where  $g(x, y)$  denotes the original image intensity,  $g_{\min}$  represents the minimum value,  $g_{\max}$  represents the maximum value,  $f(x, y)$  represents the output image with a minimum level of  $g_{\text{LIR}}$  and a maximum level of  $g_{\text{HIR}}$ . The mean intensity of the cerebrospinal fluid is used to set  $g_{\max}$ , and the mean intensity of the sinuses to set  $g_{\min}$ . It was shown in [23] that this normalization method allows for meaningful comparisons between brain MR images acquired at different times.

#### D. Amplitude-Modulation Frequency-Modulation (AM-FM) Methods

Over each segmented region, a multiscale AM-FM representation (see [17], [18]) was computed using the following equation:

$$I(x, y) = \sum_{n=1}^M a_n(x, y) \cos \varphi_n(x, y) \quad (2)$$

where  $n = 1, 2, \dots, M$  denote different scales,  $(x, y)$  define the spatial coordinates,  $a_n$  denote slowly varying instantaneous-amplitude (IA) functions and  $\varphi_n$  denote the instantaneous-phase (IP) functions. In this paper, the low, medium, and high scales were considered ( $M = 3$ ). Here, the FM components  $\cos \varphi_n$  capture fast-changing texture components. The IA can be used to quantify the contributions from each component. The instantaneous frequency (IF) functions are defined in terms of the gradient of the phase.

AM-FM demodulation was applied over a dyadic filterbank (see Fig. 3) after prefiltering using an extended 2-D Hilbert filter. Let  $I_{\text{AS}}$  be  $I_{\text{AS}} = I + j\text{H}_{2\text{-D}}\{I\}$ , where  $\text{H}_{2\text{-D}}$  denotes the 2-D Hilbert operator described in [18]. The 2-D Hilbert operator is simply the standard 1-D Hilbert operator operating along the columns of the image.

The bandpass filters were grouped into low (L), medium (M), and high (H) components (see Fig. 3). For sampling at 2.226 pixels/mm, multiplying the discrete spatial frequencies by  $2.226/(2\pi)$  converts them (componentwise) into cycles per

millimeter. To see this, note that the  $\pi$ -frequency produces samples of 1, -1, 1, -1, ... at 0.5 cycles/pixel. For the low frequencies, we have discrete frequencies from the minimum IF magnitude of  $(0, \pi/8)$  corresponding to 0.1391 cycles/mm, and to a maximum IF magnitude of  $(\pi/4, \pi/4)$  at 0.3935 cycles/mm. For the medium frequencies, we have the minimum at  $(0, \pi/4)$  corresponding to 0.2782 cycles/mm, and a maximum at  $(\pi/2, \pi/2)$  corresponding to 0.7870 cycles/mm. For the high frequencies, we have the minimum frequency at  $(0, \pi/2)$  corresponding to 0.5565 cycles/mm, and a maximum of  $(\pi, \pi)$  at 1.5740 cycles/mm.

In the multiscale AM-FM decomposition, a single AM-FM component is extracted from each scale. This is accomplished in a two-step process. First, at every pixel, AM-FM component estimates generated from each bandpass filter is estimated. Then, at every pixel, for each scale, the AM-FM component estimates that gave the largest IA estimate are selected. In other words, the low-scale component is formed by collecting the dominant, low-scale bandpass pixel estimates over the segmented ROI. A similar approach is followed for the medium and high frequency scales. A summary of how AM-FM components are estimated from each channel filter is given in the following.

Let  $\hat{f}_{\text{AS}}$  denote the output of one of the bandpass filters. The IA and IP are estimated using the following equation [17], [18]:

$$a(x, y) = |\hat{f}_{\text{AS}}(x, y)| \quad (3)$$

and

$$\varphi(x, y) = \arctan \left( \frac{\text{imag}(\hat{f}_{\text{AS}}(x, y))}{\text{real}(\hat{f}_{\text{AS}}(x, y))} \right). \quad (4)$$

The IF is computed using a variable-spacing, local phase (VS-LLP) method as described in [17] and [18] from the following:

$$\frac{d}{dx} \phi(x, y) \cong \frac{1}{n_1 \delta x} \cos^{-1} \left( \frac{g(x + n_1 \delta x, y) + g(x - n_1 \delta x, y)}{2g(x, y)} \right) \quad (5)$$

where  $g(x, y) = \hat{f}_{\text{AS}}(x, y)/|\hat{f}_{\text{AS}}(x, y)|$ , and similarly for the second component of the instantaneous frequency. In (5),  $n_1$  is an integer and  $\delta x$  refers to the sampling period along the  $x$ -coordinate direction.

For each lesion, for each frequency-scale band, 32-bin histograms of the dominant IA, IF magnitude ( $|\text{IF}|$ ), and IF angle components are computed. For the IA features, the terms low-IA, medium-IA, and high-IA refer to IA estimates derived from the different frequency scales. For the IF, the terms low-IF, medium-IF, and high-IF to refer to the derived IF magnitude estimates. The IF magnitude estimates are then normalized to cycles per millimeter, providing a physically meaningful interpretation of the texture measurements. For the low, medium, high frequency scales, the following AM-FM histogram combinations are used: 1) IA only; 2) IF magnitude ( $|\text{IF}|$ ) only; 3) IA and  $|\text{IF}|$  together; 4)  $|\text{IF}|$  and IF angle together; and 5) IA,  $|\text{IF}|$ , and IF angle together.

Here, recall that 32 bins for each histogram were used. As an example, when using IA and  $|\text{IF}|$  together, a total of 64 bins for the histograms of the IA and the  $|\text{IF}|$  was achieved.

Furthermore, note that the combination of IA and  $|IF|$  (see case 3)) includes case 1) (IA only) and case 2) (IF magnitude only). When considering combinations of these histogram features, redundancy needs to be avoided. Therefore, in this example, the combination of 1) + 3) or 2) + 3) will never be considered. Instead, the nonredundant combinations of 1) + 2) and 1) + 4) are the only ones to consider.

More generally, AM-FM models and methods have been used in a variety of image- and video-processing applications. Applications include image reconstruction [16], image retrieval [25], and video motion analysis [26]. A theoretical framework for understanding the role of multidimensional frequency modulation was reported in [27]. Christodoulou *et al.* [28] compared AM-FM texture features with classical texture features for the classification of carotid plaque ultrasound images. The study involved the use of 274 images (see also [29], 137 asymptomatic subjects and 137 patients). It was shown that the AM-FM texture features provide better results than the classical texture features. The best results were obtained when there was a combination of AM-FM scales, reaching a classification success rate of 71.5%.

#### E. Statistical Analysis

The Mann-Whitney rank-sum test (for independent samples of different sizes) [30] was used in order to identify if there are significant differences (S) or not (NS) between the extracted AM-FM features. For significant differences,  $p < 0.05$  is required for comparisons between different groups of subjects. The median values over the segmented components are used for investigating the relationships between the 0 and the 6–12 months intervals. Similarly, for comparing independent samples from equal populations, the Wilcoxon rank-sum test is used [31]. This was also done for normalized image-intensity histograms.

For independent samples of different sizes, the Mann-Whitney rank-sum test is used for detecting AM-FM feature differences between NWM, NAWM, and lesions for patients with an EDSS  $\leq 2$  and EDSS  $> 2$ , two years after the initial MRI examination. Box plots were used to compare the AM-FM features between the NAWM and lesions, both at 0 and 6–12 months.

#### F. Classification and Support Vector Machines

Classification analysis was carried out to classify brain MS lesions delineated on the baseline MRI scans into two classes according to the EDSS score that each patient was allocated two years following initial diagnosis: 1) MS patients with EDSS  $\leq 2$  and 2) in MS patients with an EDSS  $> 2$ . Here, recall that the EDSS assessment was performed two years following initial diagnosis (time 0). Thus, the classification goal was to differentiate between lesions that led to early (EDSS  $\leq 2$ ) and advanced disease cases (EDSS  $> 2$ ).

As discussed in Section II-D, there are five nonredundant histogram feature combinations for the low, medium, and high scales. Thus, there are 15 ( $5 \times 3$ ) independent classifiers that were tested. Each classifier was implemented using support vector machines (SVMs). Here, each SVM uses quadratic kernels [32] expressed as  $k(x_i, x_j) = (x_i \cdot x_j)^n$ , where  $x_i$  and  $x_j$  are

the data points and  $n = 2$ . The area under the ROC curve (AUC) is used for classifier selection. The classifier-selection rule is simple. Only classifiers that give more than an AUC of 0.5 are considered for the multiclassifier system. They are then combined using a simple majority rule.

### III. RESULTS

#### A. AM-FM Decomposition and Feature Examples

Two AM-FM decomposition examples are presented in Fig. 4. The AM-FM decomposition images were estimated for four brain lesions from two patients: 1) two brain lesions from a man in his early 50s with an EDSS score of 1 and 2) two brain lesions from another man in his early 50s with an EDSS score of 4. Here, please recall that the EDSS score was obtained two years after time zero. The goal here is to identify AM-FM texture features that can be used to differentiate between brain lesions that are associated with future EDSS scores of EDSS  $\leq 2$  and EDSS  $> 2$ . It should also be noted that the brain lesions, presented in Fig. 4, represent selected lesions extracted from the two subjects (and are not representative of the whole dataset).

The original brain lesions are given in the top row of Fig. 4. The low-, medium-, and high-frequency-scale features are given in rows (b)–(d) (see caption for details). It is interesting to note significant differences in the distribution of IA between the left-half and right-half brain lesion plots. For all scales, for the advanced cases (right-half plots), the central portions of the brain lesions give significantly lower IA values than what the corresponding values for the early disease cases (left-half plots). The IF magnitude and FM reconstruction plots for the advanced disease lesions also appear to exhibit much finer granularity than for the early disease lesions. There is clearly much more uniformity in the left-half plots as opposed to the right-half plots. The lack of AM-FM feature uniformity appears to be a characteristic of the disease.

Fig. 5 presents the box plots for the medium-frequency-scale IA and IF magnitude for all subjects investigated ( $N = 38$ ). There are also significant differences in the box plots of Fig. 5. From the plots of Fig. 5(a), a significant increase in the median IA can be seen, when comparing NWM to NAWM. On the other hand, there is also a significant decrease in IF magnitude, between NWM and NAWM. The situation is reversed in the plots of Fig. 5(b). Here, there is a significant decrease in the IA between sinuses and brain lesions. The median IF magnitude shows the opposite trend; it increases. In terms of brain lesion progression, it is interesting to note an increase in median IA accompanied by a decrease in IF magnitude. As will be discussed later in Section III-C, the medium-scale IA histogram gave excellent classification results.

#### B. Statistical Analysis

Table I presents the statistical analysis results between NAWM and the brain lesions recorded at 0 and 6–12 months, as well as between MS patients and healthy volunteers. Here, the primary goal is the detection of significant changes in the IA and IF components among the normal, normal-appearing,

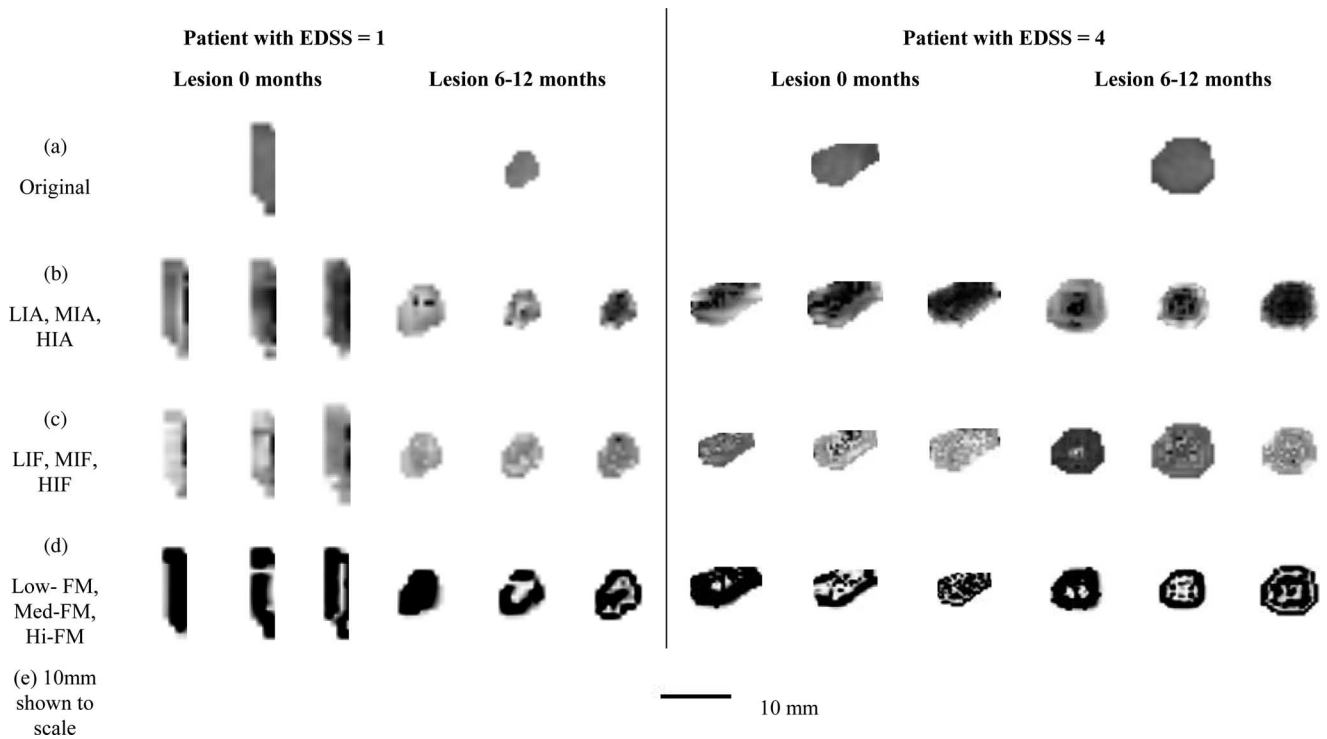


Fig. 4. Multiscale AM-FM analysis for MS brain lesions. The low-(L), medium-(M), and high-(H) frequency scales are given in columns. Four MS lesions imaged at 0 and 6–12 months are shown: one from a 51-year-old male with EDSS = 1 (left) and one from another male of similar age with EDSS = 4. (a) Original lesions. (b) Logarithmic views of the IA. (c) IF magnitude ( $|IF|$ ) of the lesions. (d) FM reconstructions of the lesions. Note that IF estimates with magnitudes outside the support of the low-, medium-, and high-scale passbands are presented in black. Thus, we only display high-confidence estimates in this Figure. The images were acquired at 2.226 pixels/mm. Also, note that the EDSS scores we assessed two years after the initial exam (0 months time point).

and diseased tissue. For NWM versus NAWM at 0 and 6–12 months, all studied components demonstrated significant differences. For NWM versus lesions at 0 and 6–12 months, all components except HIF gave significant differences. For the NAWM at 0 and 6–12 months versus lesions at 0 and 6–12 months, the low- and medium-frequency IA showed consistently significant differences. Only the medium-frequency IA component differed significantly between lesions at 0 months and lesions at 6–12 months, while only the low IF component managed to statistically resolve temporal differences for NAWM.

Table II presents the statistical comparisons for NAWM and brain lesions recorded at 0 and 6–12 months between patients allocated an EDSS score lower than or equal to 2.0 ( $\leq 2.0$ ) and patients acquiring an EDSS score greater than 2.0 ( $> 2.0$ ). It is shown that for NAWM at 0 months, there is significant difference for patients with EDSS  $\leq 2$  versus those with EDSS  $> 2$ , for the low-, medium-, and high-frequency IA, whereas for 6–12 months, there is significant difference only for the medium IA. Regarding lesions, between the two patient groups, significant differences were seen for the medium-IA and the high-IA components at both 0 months and at 6–12 months. Also, for patients acquiring an EDSS  $\leq 2$ , the medium IA component showed a statistically significant temporal dependency.

### C. Brain Lesion Classification Using AM-FM Features

Results from the independent frequency-scale histogram classifiers are presented in Table III. The best results from com-

binning the individual frequency-scale histogram classifiers are given in Table IV. Here, recall that the goal is to differentiate baseline MRI lesions between patients that ended up with an EDSS  $\leq 2.0$  from patients that gave EDSS  $> 2.0$  (two years later).

In Table III, classification results are presented in terms of sensitivity (Sen.), specificity (Sp.), correct classification rate (CR, fraction of lesions correctly classified (max = 1.0)), and AUC. The AUC is used for selecting the best AM-FM histogram features. Among the individual AM-FM histogram classifiers, the medium-frequency IA gave the best results (AUC = 0.76). It is noted that the medium-frequency-IA classifier is part of the best multiclassifier systems given in Table IV. It is also interesting to note that when the low- or the high- frequency features are used, the IA is always used. Furthermore, the low-frequency IA histogram is always used in the best multiclassifier systems of Table IV.

In terms of the correct CR, the best results were given by two different multiclassifier systems, each giving a correct CR of 0.86. Both cases include the classifier that uses all histograms from the low-frequency-scale- (IA& $|IF|$ &IF angle) and the classifier that uses the medium-frequency-scale IA histogram. The only difference between them comes from either including the IF angle (as in IA& $|IF|$ &IF angle) or excluding it (as in IA& $|IF|$  only). The use of the IF angle gave a sensitivity of 0.71 and specificity of 0.95. The exclusion of the IF angle gave a sensitivity of 0.79 and a specificity of 0.90. In terms of sensitivity, it is interesting to note that a sensitivity of 0.86 (specificity =

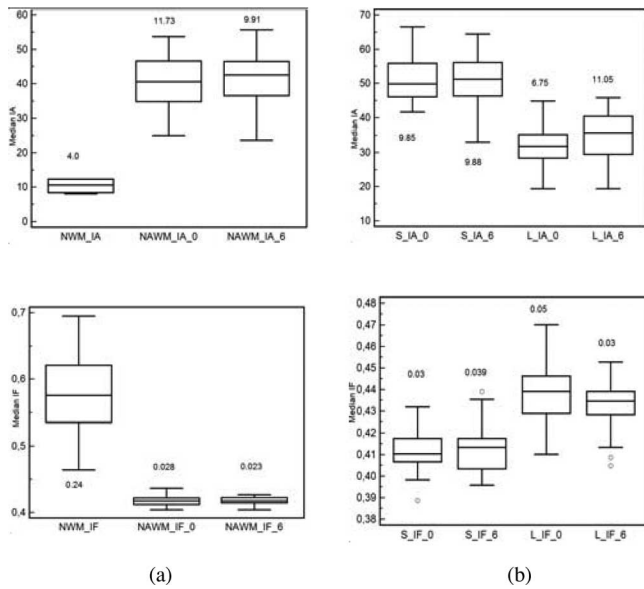


Fig. 5. Box plots for the medium-frequency-scale IA and IF magnitudes for all subjects investigated ( $N = 38$ ). From each patient, we extract the median values of the IA and the IF over all the ROIs (not to be confused with the medium-frequency scale). The box plots represent the distributions of the median values. We have the medium-scale IA (MIA) plots in the top row and the medium-scale IF magnitude in the bottom row. (a) Top figure box plots of the distribution of the median IA for the NWM and the NAWM at 0 and 6–12 months (NWM\_IA, NAWM\_IA\_0, NAWM\_IA\_6). Bottom figure box plots of the distribution of the median IF magnitude for the NWM and NAWM at 0 and 6–12 months (NWM\_IF, NAWM\_IF\_0, NAWM\_IF\_6). (b) Top figure plots of the distribution of the median IA values for the sinuses (S\_IA\_0, S\_IA\_6) and the lesions (L\_IA\_0, L\_IA\_6) at 0 and 6–12 months. The bottom figure shows the distribution of the median IF magnitude plotted for the sinuses (S\_IF\_0, S\_IF\_6) and the lesions (L\_IF\_0, L\_IF\_6) at 0 and 6–12 months, respectively. Interquartile range (IQR) values are shown above or below the box plots. In each plot, we display the median, lower, and upper quartiles and confidence interval around the median. Straight lines connect the nearest observations within 1.5 of the IQR of the lower and upper quartiles. Unfilled circles indicate possible outliers with values beyond the ends of the  $1.5 \times \text{IQR}$ . The IF magnitude is expressed in cycles per millimeter.

0.81) was obtained by simply using the low-scale IA&|IF| with the medium-scale IA.

In terms of execution times, the SVM classification algorithms were tested using a Pentium IV (2.8-GHz with 3.5-GB RAM, Microsoft Windows XP Professional, version 2002, service pack 3). Training and testing takes 12.8 s per classifier. The multiclassifier system only required 0.063 s to select through the best single classifiers and test them.

#### IV. DISCUSSION AND FUTURE WORK

The objective of this study was to investigate whether changes in AM-FM characteristics can be associated with MS disease progression. AM-FM features were extracted and investigated based on statistical measures and univariate statistical analysis. Image analysis is based on the manually segmented MS lesions from the MRI scans of the brain of 38 subjects with CIS, and the NAWM areas from the same MRI scans of the brain of the same patients were used in an attempt to quantify pathological changes that occur in MS. The population sample used in our study represents more than 50% of CIS cases diagnosed in

TABLE I

STATISTICALLY SIGNIFICANT DIFFERENCES BETWEEN AM-FM FEATURES EXTRACTED FROM THE NWM, NAWM, AND BRAIN LESIONS. WE ANALYZE THE LOW-, MEDIUM-, AND HIGH-FREQUENCY-SCALE IA AND |IF| (IA/IF). HERE, WE ARE USING THE WILCOXON RANK-SUM TEST AT  $p < 0.05$ . SIGNIFICANT DIFFERENCE IS DEPICTED WITH THE NAME OF THE COMPONENT, WHEREAS “-” DENOTES NO SIGNIFICANT DIFFERENCE

	NAWM		Lesions	
	0 months	6-12 months	0 months	6-12 months
NWM	LIA/LIF MIA/MIF HIA/HIF	LIA/LIF MIA/MIF HIA/HIF	LIA/LIF MIA/MIF HIA/-	LIA/LIF MIA/MIF HIA/-
NAWM	0 months	-/LIF -/- -/-	LIA/- MIA/- -/HIF	LIA/- MIA/- -/-
	6-12 months		LIA/LIF MIA/- -/-	LIA/LIF MIA/- -/HIF
Lesions				-/ MIA/- -/-
	0 months			-/ MIA/- -/-

NWM: Normal white matter; NAWM: normal-appearing white matter; LIA, MIA, and HIA: low, medium, and high instantaneous amplitude. LIF, MIF, and HIF: low-, medium-, and high-instantaneous-frequency magnitude.

TABLE II

COMPARISON FOR THE LOW, MEDIUM AND HIGH-FREQUENCY-SCALE IA AND |IF| (IA/IF) COMPONENTS BETWEEN PATIENTS WITH EDSS  $\leq 2$  AND EDSS  $> 2$  BASED ON THE WILCOXON RANK-SUM TEST AT  $p < 0.05$ . SIGNIFICANT DIFFERENCE IS DEPICTED WITH THE NAME OF THE COMPONENT, WHEREAS “-” DENOTES NO SIGNIFICANT DIFFERENCE. THE NUMBER OF SUBJECTS WITH EDSS  $\leq 2$  AND EDSS  $> 2$  WERE 23 AND 15, RESPECTIVELY

		NAWM		
		0 months	6-12 months	
NAWM	0 months	EDSS $> 2$	LIA/- MIA/- HIA/-	-/ -/ -/-
		EDSS $\leq 2$		
	6-12 months	EDSS $> 2$	-/ -/- -/-	-/ MIA/- -/-
		EDSS $\leq 2$		

		Lesions		
		0 months	6-12 months	
Lesions	0 months	EDSS $> 2$	-/ MIA/- HIA/-	-/ MIA/- -/-
		EDSS $\leq 2$		
	6-12 months	EDSS $> 2$	-/ -/- -/-	-/ MIA/- HIA/-
		EDSS $\leq 2$		

NWM: Normal white matter; NAWM: normal-appearing white matter; LIA, MIA, and HIA: low, medium, and high IA; LIF, MIF, and HIF: low, medium, and high IF magnitude.

the Cypriot population within the time span of two years. All subjects were scanned twice with an interval of 6–12 months.

The results indicate that several AM-FM features can be used to differentiate between brain lesions that lead to minimal (EDSS  $\leq 2.0$ ) and mild clinical signs (EDSS  $> 2.0$ ). The IA histograms from all frequency scales contributed to a multiclassifier system that gave 86% correct CR. The best classifier results also used the IF magnitude from both the low- and the high-frequency scales. It was shown from the results of Table II that both the medium-frequency-scale and high-frequency-scale IAs also gave significant differences between the two cases

TABLE III

CLASSIFICATION RESULTS USING THE SVM CLASSIFIER IN TERMS OF SENSITIVITY (SEN.), SPECIFICITY (SPC.), AUC, AND CR USING LOW-, MEDIUM-, AND HIGH-FREQUENCY COMPONENTS FOR DIFFERENTIATING LESIONS AT 0 MONTHS BETWEEN PATIENTS WITH EDSS  $\leq 2$  AND EDSS  $> 2$ . AUC VALUES BIGGER THAN 0.5 ARE GIVEN IN BOLD FACE

Feature	Low					Medium					High				
	IA	IF	IA& IF	IF &IF angle	IA& IF &IF angle	IA	IF	IA& IF	IF &IF angle	IA& IF &IF angle	IA	IF	IA& IF	IF &IF angle	IA& IF &IF angle
	Histograms														
Sen.	<b>0.71</b>	<b>0.79</b>	<b>0.71</b>	<b>0.86</b>	<b>0.79</b>	<b>0.79</b>	0.64	<b>0.71</b>	0.57	<b>0.79</b>	0.64	0.64	<b>0.79</b>	0.64	<b>0.79</b>
Spc.	<b>0.52</b>	<b>0.62</b>	0.29	0.43	0.33	<b>0.57</b>	<b>0.52</b>	<b>0.52</b>	0.38	<b>0.57</b>	0.48	0.33	0.43	0.33	0.38
AUC	<b>0.67</b>	<b>0.68</b>	<b>0.52</b>	<b>0.61</b>	<b>0.61</b>	<b>0.76</b>	<b>0.55</b>	<b>0.65</b>	<b>0.53</b>	<b>0.69</b>	<b>0.53</b>	0.46	<b>0.52</b>	0.48	<b>0.61</b>
CR	<b>0.60</b>	<b>0.69</b>	0.46	<b>0.60</b>	0.51	<b>0.66</b>	0.57	<b>0.60</b>	0.46	<b>0.66</b>	0.54	0.46	0.57	0.46	0.54

IA: Instantaneous amplitude; IF: instantaneous-frequency magnitude.

TABLE IV

BEST BRAIN LESION CLASSIFICATION RESULTS FOR DIFFERENTIATING BETWEEN CASES OF EDSS  $\leq 2$  VERSUS EDSS  $> 2$  AFTER COMBINING THE INDEPENDENT HISTOGRAM CLASSIFIERS FROM TABLE III USING A VOTING SYSTEM. WE EXAMINED ALL POSSIBLE VOTING COMBINATIONS FOR AUC LARGER THAN 0.5. WE PRESENT THE BEST FINAL RESULTS IN TERMS OF THE CORRECT RATE (CR). FOR EACH RESULT, WE ALSO PRESENT THE SENSITIVITY (SEN.) AND SPECIFICITY (SPC.) VALUES. WE SHOW FOR EACH SCALE WHICH FEATURES WERE USED. WE USE “-” TO INDICATE THAT A SCALE WAS NOT USED. HERE, WE USE A COMMA “,” TO INDICATE THAT WE ARE COMBINING INDEPENDENT SVM CLASSIFIERS. THUS, “IA, |IF|” REFERS TO THE COMBINATION OF TWO DIFFERENT CLASSIFIERS. IN CONTRAST, WE USE “&” TO INDICATE THAT WE ARE CONSIDERING THE CONCATENATION OF HISTOGRAMS INTO A SINGLE AM-FM FEATURE. THUS, “IA&|IF|&IF ANGLE” REFERS TO THE SINGLE SVM CLASSIFIER THAT COMBINES THE HISTOGRAMS FROM THE IA, |IF|, AND IF ANGLE

Sen.	Spc.	CR	Scales		
			Low	Medium	High
0.71	0.86	0.80	IA& IF &IF angle	IA	IA
0.86	0.81	0.83	IA,  IF	IA	-
0.79	0.86	0.83	IA,  IF &IF angle	IA	-
0.79	0.90	0.86	IA& IF &IF angle	IA	IA& IF
0.71	0.95	0.86	IA& IF &IF angle	IA	IA& IF &IF angle

IA: Instantaneous amplitude, IF: Instantaneous frequency.

(EDSS  $\leq 2$  versus EDSS  $> 2$ ). Among all AM-FM features, the medium-frequency-IA histogram alone gave the best AUC results (AUC = 0.76 in Table III).

It is shown from Table II that the medium-frequency-scale IA can reliably differentiate between NAWM associated with mild and advanced cases of the disease. Here, there are no significant differences in NAWM between mild cases collected at 0 and 6–12 months. Similarly, the same observations apply for the NAWM at 6–12 months (advanced cases).

NWM, NAWM, and brain lesions give AM-FM features with significant differences. As an example, consider the case of comparing NWM and NAWM at 6–12 months. This case is shown in the first row, second column of the Table I. Here, the low-frequency, medium-frequency, and/or high-frequency IA values can be used to differentiate between NWM and NAWM at 6–12 months. Similarly, one can alternatively use low-frequency,

medium-frequency IF, or high-frequency IF to differentiate between NWM and NAWM at 6–12 months. The combination of these findings suggests that AM-FM features can be used to reliably detect advanced stages of the disease. Furthermore, it was shown (see second row, second column of Table I), that the low-frequency component (LIF) can differentiate between NAWM at early (0 months) and NAWM at advanced (6–12 months) stages of the disease. The components LIA and MIA can differentiate between NWM and NAWM (both at 0 and 6–12 months) versus lesions at both 0 and 6–12 months. Furthermore, the component MIA can differentiate between lesions at 0 versus 6–12 months.

#### A. General Discussion

Various studies have been performed in order to establish a relationship between various gray levels and texture features [3]–[12]. It was shown in [3] that histograms could characterize changes between MS lesions and NAWM. It was also shown in this study that texture features and histograms may be used in discriminating between segmented areas of normal and abnormal brain tissues.

#### B. Study Limitations

The MRI images in this study were intensity-normalized based on the method proposed in [23]. This was done in order to reduce the effects of image-intensity variation between images obtained at different time points. The variation in intensity can have a significant impact when trying to compare between different images and also when trying to generate global tissue models for tissue classification [8]. The normalization process proposed in this study uses prior knowledge of the high- and low-intensity values of the brain so that the new intensity histogram of the lesion has its maximum peak close to its average gray-scale value [15].

T2-weighted MRI is very sensitive to tissue abnormalities in human brain, and many histopathological features in MS, such as edema, gliosis, demyelination, and remyelination, are depicted as hyperintensity lesions. It is not sensitive, however, to discrete tissue damage in NAWM. Since the assessment of NAWM may provide more information concerning disease

burden and evolution, the intention here was to characterize NAWM by using AM-FM features.

The fact that ROI-specific findings were summed up per subject is a limitation of the current study, since statistical results may have been distorted to some extent (either by masking differences via averaging out subtle changes or by enhancing small differences through outlier overweighting). More than two time points for imaging data acquisition would be needed to allow drawing of reliable conclusions regarding the existence or not of temporal resolving power of the features computed. In addition, the interval between the examined time points can be considered relatively small with respect to disease evolution in CIS. Although a standardized procedure was followed for brain MRI planning purposes, image registration between serial scans was not implemented to ensure maximum compatibility regarding lesion detection and segmentation. Only one observer was used for ROI delineation and, therefore, no conclusions can be drawn with regard to reproducibility or interobserver variability. Regarding texture analysis, the correspondence between texture features and histological parameters remains a matter of debate, since MRI image voxel resolution is much lower than the resolution in histological structures [7]. In addition, AM-FM analysis presented in this study is dependent [7] on: 1) MR acquisition parameters; 2) the quality assessment of the MRI device used; and 3) the methods of image reconstruction and processing.

### C. Future Directions

MRI analysis has become a powerful tool in the diagnosis of brain disease [1]–[9]. Pixel intensity variations between the same and consecutive MRI scans, i.e., intrascan and interscan variations, complicate the method of quantitative MRI analysis [8]. Improvements in the measurement and preprocessing of the image may, therefore, have a significant impact in the clinical diagnosis, image analysis, and computer-aided diagnosis. The simple method of histogram-intensity normalization proposed in [23] can help in this direction; however, more studies with larger datasets are required. This will enable an accurate computation of texture features that may provide information for better and earlier differentiation between NAWM and MS lesions and in assessing disease progression.

Further research work on a larger number of subjects is required for validating the results of this study and for finding additional AM-FM texture features that may provide information to differentiate between NAWM and MS lesions, as well as for longitudinal monitoring of these lesions. In addition, the proposed methodology could be possibly used for the assessment of subjects at risk of developing future neurological events and disease progression as measured by increased EDSS score. The extracted AM-FM features could possibly offer additional information of not yet developed lesions. Future studies might usefully investigate whether the abnormalities of the AM-FM parameters are predictive of the clinical course (through follow-up). It would also be useful to explore in more detail, the relationship between specific AM-FM parameters abnormalities and microscopic pathological abnormalities.

### REFERENCES

- [1] F. Fazekas, F. Barkhof, M. Filippi, R. I. Grossman, D. K. B. Li, W. I. McDonald, H. F. McFarland, D. W. Paty, J. H. Simon, J. S. Wolinsky, and D. H. Miller, "The contribution of magnetic resonance imaging to the diagnosis of multiple sclerosis," *Neurology*, vol. 53, pp. 448–456, 1999.
- [2] M. Filippi, D. W. Paty, L. Kappos, F. Barkhof, D. A. Compston, A. J. Thompson, G. J. Zhao, C. M. Wiles, W. I. McDonald, and D. H. Miller, "Correlations between changes in disability and T2-weighted brain MRI activity in multiple sclerosis: A follow-up study," *Neurology*, vol. 45, pp. 255–260, 1995.
- [3] J. Dehmshki, G. J. Barker, and P. S. Tofts, "Classifications of disease subgroups and correlation with disease severity using magnetic resonance imaging whole-brain histograms: Application to magnetization transfer ratios and multiple sclerosis," *IEEE Trans. Med. Imag.*, vol. 21, no. 4, pp. 320–331, Apr. 2002.
- [4] D. H. Miller, R. I. Grossman, S. C. Reingold, and H. F. McFarland, "The role of magnetic resonance techniques in understanding and managing multiple sclerosis," *Brain*, vol. 121, no. 1, pp. 3–24, Jan. 1998.
- [5] F. Barkhof, "The clinico-radiological paradox in multiple-sclerosis revisited," *Curr. Opin. Neurol.*, vol. 15, no. 3, pp. 239–245, Jun. 2002.
- [6] K. O. Lövgren, N. Anzalone, A. Dörfler, M. Essig, B. Hurwitz, L. Kappos, S. K. Lee, and M. Filippi, "MR imaging in multiple sclerosis: Review and recommendations for current practice," *Amer. J. Neuroradiol.*, vol. 31, no. 6, pp. 983–989, Jun. 2010.
- [7] S. Herlidou-Même, J. M. Constans, B. Carsin, D. Olivie, P. A. Eliat, L. Nadal-Desbarats, C. Gondry, E. Le Rumeur, I. Idy-Peretti, and J. D. de Certaines, "MRI texture analysis on texture test objects, normal brain and intracranial tumors," *Mag. Reson. Imag.*, vol. 21, pp. 989–993, 2003.
- [8] O. Yu, Y. Mauss, G. Zollner, I. J. Namer, and J. Chambron, "Distinct patterns of active and non-active plaques using texture analysis of brain NMR images in multiple sclerosis patients: Preliminary results," *Magn. Reson. Imag.*, vol. 17, no. 9, pp. 1261–1267, 1999.
- [9] J. Zhang, L. Tong, L. Wang, and N. Li, "Texture analysis of multiple sclerosis: A comparative study," *Magn. Reson. Imag.*, vol. 26, pp. 1160–1166, 2008.
- [10] J. M. Mathias, P. S. Tofts, and N. A. Losseff, "Texture analysis of spinal cord pathology in multiple sclerosis," *Magn. Reson. Med.*, vol. 42, no. 5, pp. 929–935, 1999.
- [11] C. P. Loizou, C. S. Pattichis, I. Seimenis, E. Eracleous, C. N. Schizas, and M. Pantziaris, "Quantitative analysis of brain white matter lesions in multiple sclerosis subjects: Preliminary findings," in *Proc. IEEE 5th Int. Conf. Inf. Techn. Appl. Biomed., ITAB*, Shenzhen, China, May 30–31, 2008, pp. 58–61.
- [12] C. P. Loizou, C. S. Pattichis, I. Seimenis, and M. Pantziaris, "Quantitative analysis of brain white matter lesions in multiple sclerosis subjects," in *Proc. 9th Int. Conf. Inform. Techn. Appl. Biomed., ITAB*, Larnaca, Cyprus, Nov. 5–7, 2009, pp. 1–4.
- [13] P. Theodorakis, D. Glotsos, I. Kalantzis, S. Kostopoulos, P. Georgiadis, K. Sifaki, K. Tsakouridou, M. Malamas, G. Delibasis, D. Cavouras, and G. Nikiforidis, "Pattern recognition system for the discrimination of multiple sclerosis from cerebral microangiopathy lesions based on texture analysis of magnetic resonance images," *Magn. Reson. Imag.*, vol. 27, pp. 417–422, 2009.
- [14] D. S. Meier and C. R. G. Guttman, "Time-series analysis of MRI intensity patterns in multiple sclerosis," *NeuroImaging*, vol. 20, pp. 1193–1209, 2003.
- [15] G. Collewet, M. Strzelecki, and F. Marriette, "Influence of MRI acquisition protocols and image intensity normalization methods on texture classification," *Magn. Reson. Imag.*, vol. 22, pp. 81–91, 2004.
- [16] V. Murray, P. Rodriguez, and M. S. Pattichis, "Robust multiscale AM-FM demodulation of digital images," in *Proc. IEEE Int. Conf. Image Process.*, Oct., 2007, vol. 1, pp. 465–468.
- [17] V. M. Murray Herrera, "AM-FM methods for image and video processing," Ph.D. dissertation, Univ. New Mexico, Albuquerque, Sep. 2008.
- [18] V. Murray, P. Rodriguez, and M. S. Pattichis, "Multi-scale AM-FM demodulation and reconstruction methods with improved accuracy," *IEEE Trans. Imag. Process.*, vol. 19, no. 5, pp. 1138–1152, May 2010.
- [19] M. S. Pattichis, "Multidimensional AM-FM models and methods for biomedical image computing," in *Proc. 34th IEEE Annu. Int. Conf. Eng. Med. Biol. Soc.*, Sep. 2–6, 2009, pp. 5641–5644.
- [20] A. J. Thompson and J. C. Hobart, "Multiple sclerosis: Assessment of disability and disability scales," *J. Neurol.*, vol. 254, no. 4, pp. 189–196, 1998.

- [21] C. P. Loizou, V. Murray, M. S. Pattichis, M. Pantziaris, and C. S. Pattichis, "AM-FM texture image analysis in multiple sclerosis brain white matter lesions," in *Proc. XII Med. Conf. Med. Biol. Eng. Comput. (Medicon 2010)*, May 27–30, Porto Caras, Greece, pp. 446–449.
- [22] C. P. Loizou, V. Murray, M. S. Pattichis, M. Pantziaris, and C. S. Pattichis, "AM-FM texture image analysis in brain white matter lesions in the progression of Multiple Sclerosis," in *Proc. IEEE Southwest Symp. Image Anal. Interpr. (SSIAI)*, May 23–25, 2010, pp. 61–64.
- [23] C. P. Loizou, M. Pantziaris, I. Seimenis, and C. S. Pattichis, "MRI intensity normalization in brain multiple sclerosis subjects," in *Proc. 9th Int. Conf. Inform. Technol. Appl. Biomed. (ITAB)*, Larnaca, Cyprus, Nov. 5–7, 2009, pp. 1–5.
- [24] M. Nixon and A. Aguado, *Feature Extraction & Image Processing*. Woburn, MA: Newnes, 2002.
- [25] V. Murray, M. S. Pattichis, and P. Soliz, "New AM-FM analysis methods for retinal image characterization," in *Proc. 42nd IEEE Asilomar Conf. Signals, Syst. and Comput.*, 2008, pp. 664–668.
- [26] V. Murray, S. Murrilo, M. S. Pattichis, C. P. Loizou, C. S. Pattichis, E. Kyriakou, and A. Nicolaides, "An AM-FM model for motion estimation in atherosclerotic plaque videos," in *Proc. 41st IEEE Asilomar Conf. Signals, Syst. and Comput.*, Nov. 4–7, 2007, pp. 746–750.
- [27] M. S. Pattichis and A. C. Bovik, "Analyzing image structure by multi-dimensional frequency modulation," *IEEE Trans. Pattern Anal. Mach. Intell.*, vol. 29, no. 5, pp. 753–766, May 2007.
- [28] C. I. Christodoulou, C. S. Pattichis, V. Murray, M. S. Pattichis, and A. N. Nicolaides, "AM-FM representations for the characterization of carotid plaque ultrasound images," in *Proc. 4th Eur. Conf. Int. Feder. Med. Biolog. Eng. (MBEC'08)*, Antwerp, Belgium, Nov. 23–28, pp. 1–4.
- [29] C. I. Christodoulou, C. S. Pattichis, M. Pantziaris, and A. Nicolaides, "Texture-Based classification of atherosclerotic carotid plaques," *IEEE Trans. Med. Imag.*, vol. 22, no. 7, pp. 902–912, Jul. 2003.
- [30] W. J. Conover, *Practical Nonparametric Statistics*, 3rd ed. New York: John Wiley & Sons, 1999.
- [31] D. G. Altman, *Practical Statistics for Medical Research*. London, U.K.: Chapman and Hall, 1991.
- [32] N. Cristianini and J. Shawe-Taylor, *An Introduction to Support Vector Machines and Other Kernel-based Learning Methods*, 1st ed. Cambridge, MA: Cambridge Univ. Press, 2000.



**C. P. Loizou** (M'05) received the B.Sc. degree in electrical engineering and the Dipl.-Ing. (M.Sc.) degree in computer science and telecommunications from the University of Kaiserslautern, Kaiserslautern, Germany, in 1986 and 1990, respectively, and the Ph.D. degree in ultrasound image analysis of the carotid artery from the Department of Computer Science, Kingston University, London, U.K., in 2005.

From 1996 to 2000, he was a Lecturer in the Department of Computer Science, Higher Technical Institute, Nicosia, Cyprus. Since 2000, he has been an Assistant Professor in the Department of Computer Science, School of Sciences and Engineering, Intercollege, Limassol, Cyprus. He was a Supervisor of a number of Ph.D. and B.Sc. students in computer image analysis and telemedicine.

He is also an Associate Researcher at the Institute of Neurology and Genetics, Nicosia, Cyprus. He is the author or coauthor of the book *Despeckle Filtering Algorithms and Software for Ultrasound Imaging*, 12 chapters in books, 13 referred journals, and 52 conference papers in image and video analysis. His research interests include medical imaging and processing, motion and video analysis, signal and image processing, pattern recognition, biosignal analysis, in ultrasound, magnetic resonance, and optical coherence tomography imaging and computer applications in medicine.

Dr. Loizou is a Senior Member of the Institution of Electrical Engineers.



**V. Murray** (M'01) received the B.S. (high honors—ranked first in the class) degree in electrical engineering from the Pontificia Universidad Católica del Perú, Lima, Perú, in 2003, and the M.S. and Ph.D. degrees in electrical engineering from the University of New Mexico (UNM), Albuquerque, in 2005 and 2008, respectively.

He is currently a Research Assistant Professor in the Department of Electrical and Computer Engineering, UNM, where he is involved in developing adaptive reconfigurable hardware, based on field-programmable gate array (FPGAs), for the Air Force Research Laboratory, and developing methods and algorithms in medical imaging for detecting diseases in human eyes for VisionQuest Biomedical, Albuquerque. His research interests include amplitude modulation–frequency modulation demodulation methods, digital image and video processing, medical imaging, and hardware design using very high descriptive language (VHDL) and FPGAs.



**M. S. Pattichis** (M'99–SM'06) received the B.Sc. (high honors and special honors) degree in computer sciences and the B.A. (high honors) degree in mathematics, the M.S. degree in electrical engineering, and the Ph.D. degree in computer engineering, in 1991, 1993, and 1998, respectively, all from the University of Texas, Austin.

He is currently an Associate Professor in the Department of Electrical and Computer Engineering, University of New Mexico (UNM), Albuquerque, where he is also an Associate Professor in the Department of Radiology. He is an Associate Editor of the *Pattern Recognition*. His research interests include digital image and video processing and communications, dynamically reconfigurable computer architectures, and biomedical and space-image-processing applications.

Dr. Pattichis is an Associate Editor of the IEEE TRANSACTIONS ON INDUSTRIAL INFORMATICS. He was the General Chair of the 2008 IEEE Southwest Symposium on image analysis and interpretation. He was a recipient of the 2004 Electrical and Computer Engineering Distinguished Teaching Award, and the 2006 School of Engineering Harrison Faculty Recognition Award at UNM.



**I. Seimenis** is a qualified medical physicist specializing in diagnostic radiology. He received the B.Sc. degree in physics from the University of Athens, Greece, in 1992, and the M.Sc. and Ph.D. degrees in medical physics from the University of Aberdeen, U.K., in 1992 and 1997, respectively.

He is currently a Medical Physicist at the Medical Diagnostic Center "Ayios Therissos," Nicosia, Cyprus. His research interests include clinical magnetic resonance imaging (MRI), computed tomography dosimetry, polymer gel dosimetry, and medical image analysis. He has been involved in numerous scientific projects in the aforementioned fields funded by the European Union (EU) and research promoting bodies in the U.K., Greece, and Cyprus. He is the author or coauthor of 33 refereed journal papers with a total impact factor of 103.



**M. Pantziaris** received the M.D. degree in neurology from the Aristotelion University, Thessaloniki, Greece, in 1995.

He was trained in Carotid Duplex–Doppler ultrasonography at St. Mary’s Hospital, London, in 1995. During 1999, he was a Visiting Doctor in acute stroke treatment at Massachusetts General Hospital, Harvard University, Boston, MA. He is currently a Senior Neurologist in the Neurological Department, Cyprus Institute of Neurology and Genetics, Nicosia, Cyprus, and is also the Head of the Neurovascular Department. He has considerable experience in carotid–transcranial ultrasound, has participated in many research projects. He is the author or coauthor of several publications. He is also the Head of the Multiple Sclerosis (MS) Clinic, where he is involved in research projects studying the etiology and therapy of MS.



**C. S. Pattichis** (S’88–M’88–SM’99) was born in Cyprus, in January 30, 1959. He received the Diploma degree in technician engineering from the Higher Technical Institute, Nicosia, Cyprus, in 1979, the B.Sc. degree in electrical engineering from the University of New Brunswick, NB, Canada, in 1983, the M.Sc. degree in biomedical engineering from the University of Texas, Austin, in 1984, the M.Sc. degree in neurology from the University of Newcastle Upon Tyne, U.K., in 1991, and the Ph.D. degree in electronic engineering from the University of London, London, U.K., in 1992.

He is currently a Professor in the Department of Computer Science, University of Cyprus, Nicosia, Cyprus. His research interests include e-health, medical imaging, biosignal analysis, and intelligent systems. He has been involved in numerous projects in these areas funded by the European Union (EU), the National Research Foundation of Cyprus, the INTERREG, and other bodies, with a total funding managed in excess of five million Euros. He was on the Editorial Board of the *Journal of Biomedical Signal Processing and Control*. He is the Co-Editor of the books: *M-Health: Emerging Mobile Health Systems* (New York: Springer, 2006), and *Information Technology in Biomedicine* (IEEE, to be published in 2010). He is the coauthor of the monograph *Despeckle Filtering Algorithms and Software for Ultrasound Imaging* (San Rafael, CA: Morgan & Claypool, 2008). He is the author or coauthor of 52 refereed journal and 142 conference papers, and 19 chapters in books in these areas.